Bulletin of the Seismological Society of America, Vol. 100, No. 5B, pp. 2574–2589, November 2010, doi: 10.1785/0120090286

Remotely Triggered Seismicity in Continental China following the 2008 M_w 7.9 Wenchuan Earthquake

by Tao Jiang, Zhigang Peng, Weijun Wang, and Qi-Fu Chen

Abstract We perform a systematic search of remotely triggered seismicity in continental China following the 2008 M_w 7.9 Wenchuan earthquake. We visually identify earthquakes as impulsive seismic energy with clear *P* and *S* arrivals on 5 Hz high-pass filtered three-component velocity seismograms 1 hr before and after the Wenchuan earthquake. Out of the 271 stations in the updated Chinese digital seismic network (CSN), 17 stations show statistically significant seismicity increase with β-statistic values larger than 2, following the Wenchuan earthquake. These include 11 stations in the north China block, which is seismically active and is in the rupture propagation direction of the Wenchuan earthquake, three stations along the coastal lines in the relatively stable south China block, one station near the Haiyuan fault zone in northwest China, and two stations near the Tanlu fault zone and the Longgang volcano in northeast China. These observations suggest that dynamic triggering in intraplate regions tends to occur near active faults that have ruptured in historic times and in the rupture propagation directions of the mainshock. However, it is worth noting that many sites that satisfy the criteria are not triggered, suggesting that these conditions would help but are not sufficient enough to guarantee remote triggering in intraplate regions. The tectonic environments near the sites with clear triggered activity range from transpressional to tranextentional, and most regions are not associated with active geothermal or volcanic activity, indicating that dynamic triggering could occur in a wide range of tectonic environments.

Online Material: Tables of station information and measured parameters and two supplementary figures showing locally triggered earthquakes.

Introduction

It is well known that earthquakes interact with each other. Large shallow earthquakes are typically followed by increased seismic activity that is termed "aftershocks" (e.g., Omori, 1894; Utsu *et al.*, 1995). Whereas aftershocks mostly occur in the immediate vicinity of the mainshock rupture zone, in recent years seismologists have found compelling evidence that large earthquakes could also cause a significant increase of seismic activity in regions that are several hundreds to thousands of kilometers away (e.g., Hill *et al.*, 1993; Anderson *et al.*, 1994; Brodsky *et al.*, 2000; Gomberg *et al.*, 2001; Hough and Kanamori, 2002; Gomberg *et al.*, 2004; Husen *et al.*, 2004; Husker and Brodsky, 2004; Pankow *et al.*, 2004; Prejean *et al.*, 2004; Brodsky and Prejean, 2005; Miyazawa and Mori, 2005; West *et al.*, 2005; Miyazawa and Mori, 2006; Hill and Prejean, 2007; Rubinstein *et al.*, 2007; Gomberg *et al.*, 2008; Miyazawa *et al.*, 2008; Miyazawa and Brodsky, 2008; Peng *et al.*, 2008; Peng and Chao, 2008; Velasco *et al.*, 2008; Peng *et al.*, 2009; Rubinstein *et al.*, 2009; Peng *et al.*, 2010). The immediate causes of these triggered events are dynamic stresses from the passing seismic waves, which can be estimated from the nearby broadband seismic recordings. Because of this, a systematic analysis of remote triggering offers a unique opportunity to better understand the physical mechanisms of earthquake interaction and nucleation.

Despite the increasing number of observations, many fundamental questions about remote triggering remain open. The first question is, "What are the necessary conditions of remote triggering?" Most previous studies have shown that dynamic triggering occurred preferentially at geothermal/volcanic regions and areas associated with extensional and transextensional environments (Hill and Prejean, 2007 and reference therein). In addition, it has been suggested that areas with higher background seismicity (e.g., active plate boundary regions or aftershock zones of previous large earthquakes) are more susceptible to dynamic triggering, most likely because these areas contain nucleation points more frequently closer to failure (e.g., Hill *et al.*, 1993; Hough *et al.*,

2003). On the other hand, recent studies have also found that dynamic triggering could occur in relatively stable regions with low background seismicity (e.g., Gomberg *et al.*, 2004; Velasco *et al.*, 2008). Finally, Harrington and Brodsky (2006) found a lack of widespread triggering in Japan with abundant background seismicity. In viewing these somewhat contradicting observations, Hill and Prejean (2007) suggested, "a systematic study of the occurrence of triggering over large areas (such as the tectonically active western United States or the more stable mid-continent) that includes more recent and complete observations is yet to be done."

The second challenging question is, "What are the physical processes responsible for triggering seismicity at teleseismic distances?" Because the identification of remotely triggered seismicity, many physical models have been proposed. These models can be largely classified into two categories (Hill and Prejean, 2007): triggered by Coulomb failure via different frictional laws (e.g., Gomberg *et al.*, 1997; Gomberg *et al.*, 2001; Perfettini *et al.*, 2003; Gomberg *et al.*, 2005; Johnson and Jia, 2005; Hill, 2008) and triggered through excitation of crustal fluids (Linde *et al.*, 1996; Brodsky *et al.*, 1998; Hill *et al.*, 2002; Brodsky *et al.*, 2003). Detailed information about the triggered earthquakes (i.e., origin times, hypocentral locations, focal mechanisms), the triggering waves and associated dynamic stresses at depth (fault orientation, depth, amplitude, and frequency), and the local conditions (tectonic environments, hydrological properties) are needed to distinguish among different models.

Here, we conduct a systematic survey of remote triggering in continental China following the 12 May 2008 M_w 7.9 Wenchuan earthquake. China situates in the southeastern part of the Eurasian plate, which is bounded by the Indian, the Philippine Sea, and the Pacific plates (e.g., Deng *et al.*, 2003; Liu *et al.*, 2007). The majority of the region belongs to the plate interior and can be classified into six fault block regions (Deng *et al.*, 2003): Tibetan plateau, Xinjiang, north China, northeast China, south China, and the south China Sea (Fig. 1). Most large earthquakes in continental China occurred along the boundaries of these active blocks (e.g., Zhang *et al.*, 2003) and are generally called intraplate earthquakes (e.g., Stein, 2007). The 2008 Wenchuan earthquake is a classic example of such an intraplate event. It ruptured ~250 km along the Longmen Shan thrust belt that bounds the Tibetan plateau and the Sichuan basin in the south China block (e.g., Burchfiel *et al.*, 2008; Xu *et al.*, 2009). The main event and its rigorous aftershock sequences were recorded continuously by many permanent and temporary seismic stations deployed by the China Earthquake Administration (CEA), providing an unprecedented seismic dataset for studying remote triggering in intraplate regions.

Peng *et al.* (2010) conducted an initial study of remotely triggered seismicity in north China associated with the 2008 Wenchuan earthquake. This study extends the analysis of Peng *et al.* (2010) to the rest regions in continental China. In addition, in this work we use an improved statistical

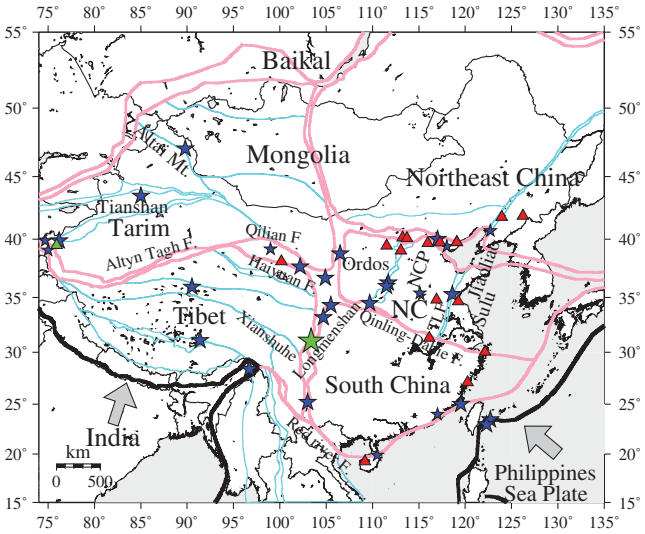

Figure 1. A summary map showing major tectonic blocks and block-boundary faults (first order: thick line, second order: thin line) in continental China (Deng *et al.*, 2003). The small stars are historical earthquakes with $M > 8$ since 1300, a few with $M > 7$ and one M 6 earthquake mentioned in the text. The large solid star marks the epicenter of the 2008 M_w 7.9 Wenchuan earthquake. The solid triangles mark the 17 stations that show significant triggering in this study. NC: north China. NCP: north China Plain. TLF: Tanlu fault. Modified from Liu *et al.* (2007). The color version of this figure is available only in the electronic edition.

method that includes the event amplitude to test the triggering significance. In the following sections, we first introduce the analysis procedure. Next, we present the results in each of the fault block region. Finally, we summarize the observations and discuss the necessary conditions that favor remote triggering and the corresponding physical mechanisms of remote triggering in intraplate regions.

Analysis Procedure

The analysis procedure generally follows that of Peng *et al.* (2010) and is briefly described in this paper. We first download continuous waveform data recorded by CSN 1 hr before and after the predicted P arrivals of the Wenchuan earthquake based on the standard iasp91 model (Kennett and Engdahl, 1991). We only examine the 1-hr data, mainly because recent studies have found that the majority of the triggered seismicity occurred during and immediately after the large surface waves (Velasco *et al.*, 2008). In addition, we only select stations with distances to the epicenter of the Wenchuan mainshock > 600 km (approximately two times the mainshock rupture length) to avoid heavily clipped signals and contaminations of strong aftershocks from the mainshock rupture region. We visually examine all the records and remove those bad traces with no seismic data or severely clipped (i.e., clipped with ~100 s or more) during the passage of the surface waves of the Wenchuan earthquake. Out of the 600 available stations, 271 stations are retained for further analysis

(Ⓔsee Table S1, available in the electronic supplement to this paper). Among them, 162 stations (60%) recorded slightly clipped signals, whereas the rest 109 stations recorded the Wenchuan earthquake onscale. Next, we apply a 5-Hz high-pass-filter to the 3-component data, smooth it with a half width of 50 points (0.5 s for 100 sample/s data), and stack the 3-component envelopes together to obtain an average envelope function for each station (Peng *et al.*, 2007; Peng *et al.*, 2010).

To evaluate the significance of seismicity rate change at each station, we compute two β-statistic values (Matthews and Reasenberg, 1988; Reasenberg and Simpson, 1992) based on the high-pass filtered envelope functions. The first automatic β-value is directly measured from the envelope functions by excluding the *P*-wave window (Miyazawa and Mori, 2005). The second manual β-value is computed based on the amplitudes of the hand-picked events. In both cases, we require the amplitudes used in the computation of the beta-statistic to be at least 10 times of the median absolute deviation (MAD) of the envelope function (Shelly *et al.*, 2007; Peng *et al.*, 2010) before the mainshock. Such criterion is applied mainly to minimize the influence of random high-frequency noise recorded by the surface stations. A detailed description on how to compute the automatic and manual β-values is given in the Appendix.

Figure 2a shows automatic β-values for all 271 stations in continental China. We find many stations with large positive β-values, especially for those near the mainshock rupture zones. A detailed examination of the high-pass filtered seismograms reveals that whereas the large positive β-values do correspond to elevated high-frequency signals after the mainshock, most of them are either associated with large early aftershocks from the mainshock rupture region or noiselike signals with no clear double picks (i.e., a hallmark of local earthquakes). Because of this, we only pick events with clear *P* and *S* arrivals and the *S-P* times are less than 15 s to ensure that the high-frequency signals are generated by local earthquakes (Ⓔsee Table S2, available in the electronic supplement to this paper) and compute the manual β-value for stations with at least one hand-picked events after the Wenchuan mainshock. We consider the triggering as statistically significant when both the automatic and manual β-values are larger than 2 (Reasenberg and Simpson, 1992; Hill and Prejean, 2007). Out of the 271 stations we have examined, 17 stations satisfy such criteria (Fig. 2b-f). To evaluate potential contaminations from random fluctuations of background seismicity, we also check the manual β-values calculated from hand-picked events within 1 to 6 hr before the mainshock (Ⓔsee Table S3, available in the electronic supplement to this paper).

Following the classifications of Deng *et al.* (2003), we divide continental China into five first-order fault bounded blocks (Figs. 1 and 2). The south China Sea block is not included because we have no waveform data in that area. In each block, we first briefly summarize the tectonic structure and historical earthquakes, followed by a detailed description of the triggered activity.

Triggered Activity in the Tibetan Plateau

The Tibetan plateau is the most active fault block region in continental China. It directly resulted from the collision of the India subcontinent with the Eurasia plate (e.g., Deng *et al.*, 2003; Avouac, 2008). Large earthquakes (e.g., $M \sim 8.0$) mainly occur on major faults that mark the boundary of the Tibetan plateau and nearby tectonic plates or blocks (Fig. 2b). These include the Himalaya thrust fault system in the south, the left-lateral Altyn Tagh, Qilian, and Haiyuan faults in the north along the northern Qilianshan-Hexi Corridor basin, and the Longmen Shan thrust belt in the east.

We find clearly triggered activity at station QH.QIL in the Qinghai province. A total of 12 events are identified from the 5-Hz high-pass filtered seismograms after the Wenchuan earthquake (Fig. 3). In comparison, no earthquakes are shown in the high-pass filtered seismograms before the mainshock. Whereas it is possible that some of the high-frequency energy bursts could be contaminated by early aftershocks around the mainshock region, we argue that most of them are associated with locally triggered seismicity because of the following two reasons. First, we only pick events with *S-P* times of less than 15 s, which corresponds to the epicentral distance of ~120 km. Station QH.QIL is located very close (within 10 km) of the Haiyuan fault zone and is at least 780 km away from Qingchuan, the northern end of the Wenchuan rupture zone near the border of the Sichuan and Gansu Provinces (Xu *et al.*, 2009). In addition, most events have clear high-frequency energy of up to 30 Hz, and some of them are large enough to be recorded by the nearby stations GS.SNT, GS.GTA, GS.SDT, GS.YJZ and GS.ZHY (Ⓔsee Fig. S1, available in the electronic supplement to this paper). Unfortunately, we do not have the seismic data before the mainshock for most of these nearby stations. Because of this, these stations are not included in final 271 stations with calculated ß-values. Nevertheless, we conclude that those high-frequency signals are most likely caused by triggered earthquakes near the Haiyuan fault zone.

As mentioned before, the Haiyuan fault zone is a major left-lateral fault system bounding the northeastern edge of the Tibetan plateau (Cavalié *et al.*, 2008). This region is seismically active, and the last major events occurred on the Haiyuan fault zone were the 1920 $M \sim 8.5$ Haiyuan and the 1927 $M \sim 8.0$ Gulang earthquakes. However, the seismicity rate from the regional catalog within 30 days of the Wenchuan earthquake is relatively low and does not show significant changes before and after the Wenchuan mainshock (with the β-value of -1.33). In addition, none of these newly identified events were listed in the local earthquake catalogs compiled by the CEA. Hence, based on catalog information alone, one could conclude that no earthquakes are triggered by the Wenchuan earthquake in this region. Instead, the β-values from the automatic and manual procedures are larger

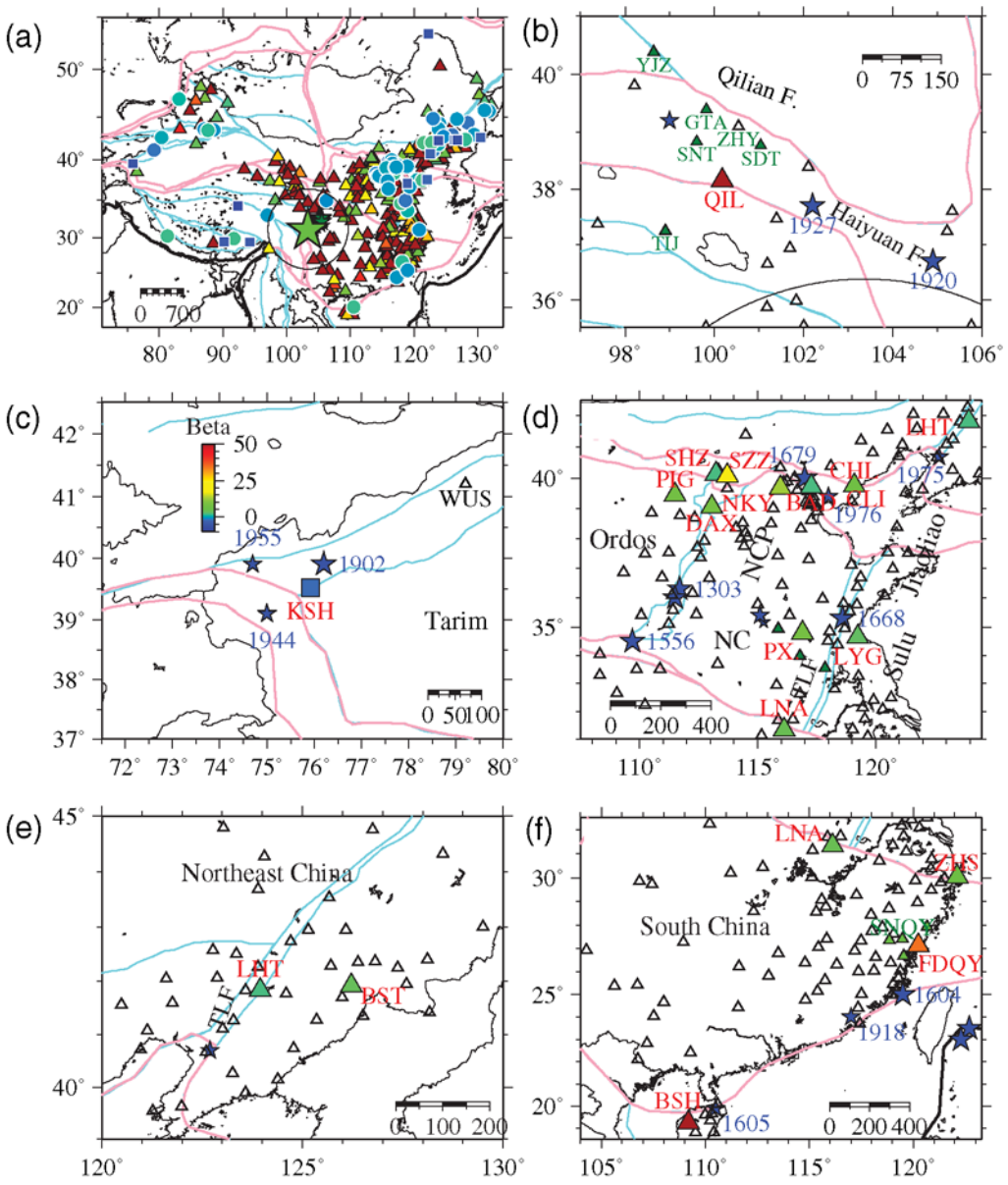

Figure 2. (a) A summary map showing all the stations coded by the automatic β-statistic values associated with the Wenchuan mainshock in continental China. The triangles mark the stations with significant triggering ($\beta \geq 2$), the circles mark the stations with $-2 < \beta < 2$, and the squares mark the stations with $\beta \leq -2$. The large solid star marks the epicenter of the M_w 7.9 Wenchuan earthquake. The black circle corresponds to the 600 km from the epicenter. (c) The coding bar is shown. (b-f) A zoom-in map around each subregion showing the seismic stations (open triangles) and those with clear triggering shaded by the β-value, major block-boundary faults (first order: thick line, second order: thin line), and historic earthquakes (stars). The filled triangles in (b) denote a few stations near the Haiyuan fault zone with seismic data only after the Wenchuan earthquake. Station names that are mentioned in the main text are also marked. The color version of this figure is available only in the electronic edition.

than 100, suggesting a significant change in seismicity rate. Prejean *et al.* (2004) found similar features in California and the Pacific Northwest after the 2002 M_w 7.8 Denali fault earthquake. These observations highlight the importance of analyzing continuous seismic recordings for studying remotely triggered earthquakes. Finally, the triggered activity near the Haiyuan fault zone (Fig. 3) is the only clear case around the Tibetan plateau. A lack of triggered activity in this region is at least partially caused by the sparse distribution of the high-quality seismic stations (Fig. 2b).

Triggered Activity in Xinjiang

The Xinjiang fault block region consists of two structurally intact Tarim and Jungar basins, and the Tianshan Mountain in between, which is a Cenozoic rejuvenated orogenic belt (Figs. 1 and 2c). We examine a total of 22 available stations and find no clear triggered activity in this region. In the following section, we show an example of a negative case at station XJ.KSH (Fig. 4) located near the Kuqa–Kashi active fault-fold zone, which is the boundary of Tianshan Mountain

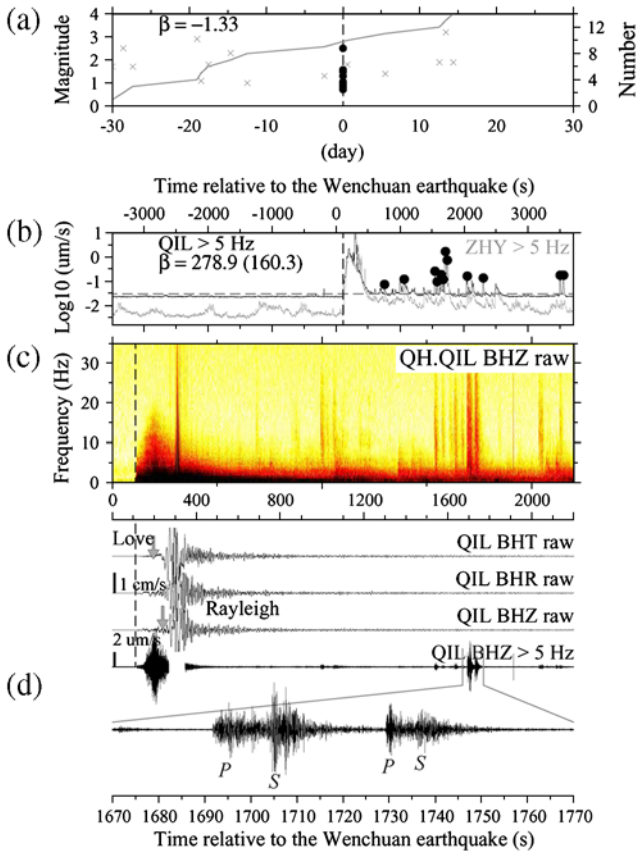

Figure 3. (a) Seismicity within 30 days of the Wenchuan mainshock and within 120 km of station QH.QIL near the Haiyuan fault zone in the northeastern boundary of the Tibetan Plateau. The crosses mark the events listed in the regional earthquake catalog, and the line shows the cumulative number of events. (b) The solid circles mark the 12 local events identified from the high-pass filtered envelopes. The corresponding β-statistic based on the catalog is −1.33. The high-pass filtered envelope functions at station QH.QIL (solid line) and the nearby station GS.ZHY (gray line) within 1 hr of the *P*-wave arrival of the Wenchuan earthquake (vertical dashed line). The open and solid circles mark the hand-picked events before and after the *P* arrival. The corresponding automatic and manual β-values are 278.9 and 160.3, respectively. The horizontal black dashed line marks the 10 × MAD threshold. (c) The spectrogram of the vertical-component seismogram recorded at station QH.QIL. We applied a 0.5 Hz high-pass filtering to the raw data before computing the spectrogram to remove the potential high-frequency artifact by computing short-time fast Fourier transform (FFT) for long-period signals. (d) Raw and high-pass filtered seismograms showing the teleseismic waves of the Wenchuan earthquake and local seismic events, respectively. The top three traces: the raw three-component (transverse, radial and vertical) seismograms recorded at station QH.QIL. The middle trace: 5 Hz high-pass filtered seismograms on vertical-component showing small local earthquakes during and immediately after the passage of surface waves. The bottom trace: a zoom-in plot of the vertical seismograms showing the *P* and *S* waves of the two triggered earthquakes recorded at station QH.QIL. The color version of this figure is available only in the electronic edition.

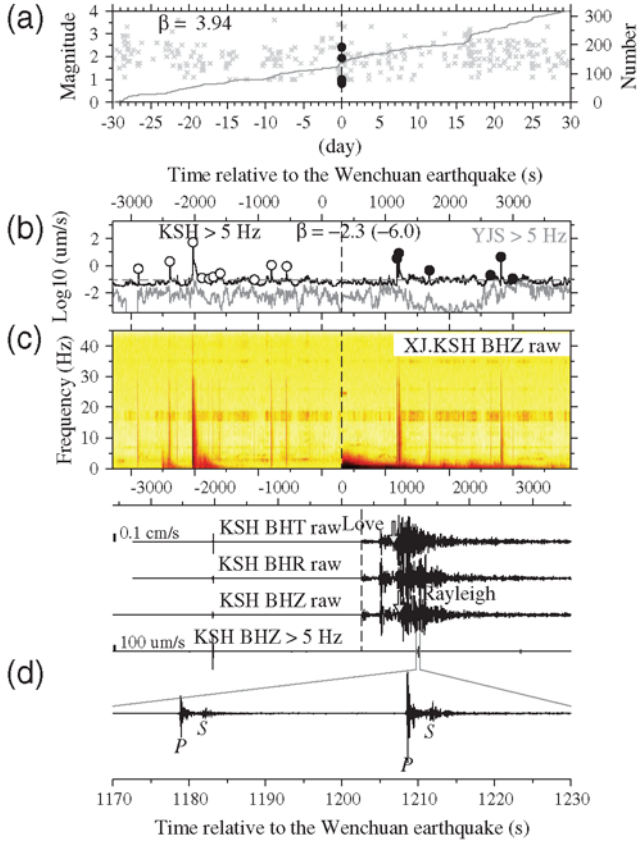

Figure 4. (a) Seismicity within 30 days of the Wenchuan mainshock and within 120 km of station XJ.KSH in Xinjiang. (b) The high-pass filtered envelope functions at station XJ.KSH (solid line) and nearby station XJ.YJS (gray line) within 1 hr of the *P*-wave arrival of the Wenchuan earthquake (vertical dashed line). (c) The spectrogram of the vertical-component seismogram recorded at station XJ.KSH. (d) Raw and high-pass filtered seismograms showing the teleseismic waves of the Wenchuan earthquake and locally generated seismic events, respectively. Other symbols and notations are the same as in Figure 3. The color version of this figure is available only in the electronic edition.

and the Tarim basin. Many large earthquakes occurred in this area since 1900. These include the 22 August 1902 $M \sim 8.3$ Atushi earthquake, with its epicenter only 49 km from station XJ.KSH; the 28 September 1944 $M \sim 7.0$ Kashi earthquake (~97 km away from XJ.KSH); and the 15 April 1955 $M \sim 7.0$ Wuqia earthquake (~112-km away).

Figure 4a shows the comparison of microseismicity within 120 km of the station XJ.KSH 30 days before and after the Wenchuan mainshock. The β-value from the regional earthquake catalog is 3.94, which would suggest that the triggering effect is significant. However, a close examination of the seismicity pattern reveals that the increasing activity is mainly associated with two swarmlike sequences, one occurred within 1 day before the mainshock, and the other one occurred 16–17 days after the mainshock. Figure 4b–d shows many small earthquakes occurred after the Wenchuan mainshock, with one M_L 1.6 event at ~1200 s that is listed in the regional earthquake catalog. However, we also identify many events within 1 hr before the mainshock, with one M_L 3.3 event occurred at −2020 s, which is also listed in the catalog. The obtained ß-values from both the automatic and manual procedures are −6.0 and −2.3, respectively. Although we

could not reliably rule out the possibility that those events around station KSH after the Wenchuan mainshock were not triggered, the fact that much more events were observed before as compared with after the mainshock suggests that they are less likely to be triggered but rather represent the ongoing swarmlike activity that started 1 day before the mainshock.

Triggered Activity in North China

In contrast to the fast crustal deformation in Tibetan plateau and Xinjiang fault block region, the deformation rate in the north China fault block is much slower, and its tectonic structure is more complex (e.g., Deng *et al.*, 2003; Liu *et al.*, 2007). It can be approximately divided into three parts (Figs. 1 and 2d). The western part is the relatively stable Ordos plateau and the surrounding rift systems. The central part is the north China plain, which is an active basin formed under pull-apart conditions and crosscut by many conjugate faults in the north-northeast and northwest-west directions (Deng *et al.*, 2003). The eastern part contains the Bohai basin and the Jiaoliao and Sulu blocks along coastal regions, which are separated from the north China plain by the Tanlu fault zone. Numerous earthquakes of size M 8 have occurred within and along the boundaries of the north China fault block. These include the 1303 Hongtong earthquake, the 1556 Huanxian earthquake, the 1668 Tancheng earthquake, and the 1679 Sanhe-Pinggu earthquakes. In addition, during the 1960s and 1970s the north China plain was seismically active with several large $M \geq 7.0$ earthquakes (including the 1975 M_w 7.0 Haicheng and 1976 M_w 7.6 Tangshan earthquakes). Because this region is heavily populated, these large intraplate earthquakes have caused significant casualties in the Chinese history (Utsu, 2002).

Out of the 77 stations available in the north China block, we find a total of 11 stations that have recorded clearly triggered activity. Some stations in the north China plain around Beijing have been reported previously (Peng *et al.*, 2010), and their results are briefly summarized here together with observations from other regions in the north China block.

Station BJ.NKY recorded one of the best examples of remotely triggered seismicity in this study (Fig. 5). This station situates ~35 km southwest of Beijing near the Babaoshan and Huangzhuang–Gaoliying faults, which mark the major boundary between the Taihang Mountain to the west and the Bohai Bay Basin to the east (Chen *et al.*, 2008). A relatively weak high-frequency signal occurred at ~390 s in the first cycle of the long-period Love waves. The strongest high-frequency signals show up between 400 and 470 s when the Love wave reaches its largest amplitude. Other bursts of high-frequency energy were initiated between 500–530 s during the large-amplitude Rayleigh waves. Because we can clearly identify the P and S waves of each event, and the S-P time is generally less than 2 s, these high-frequency energy bursts are most likely generated by locally triggered earthquakes near the subparallel Babaoshan and Huangzhuang–Gaoliying

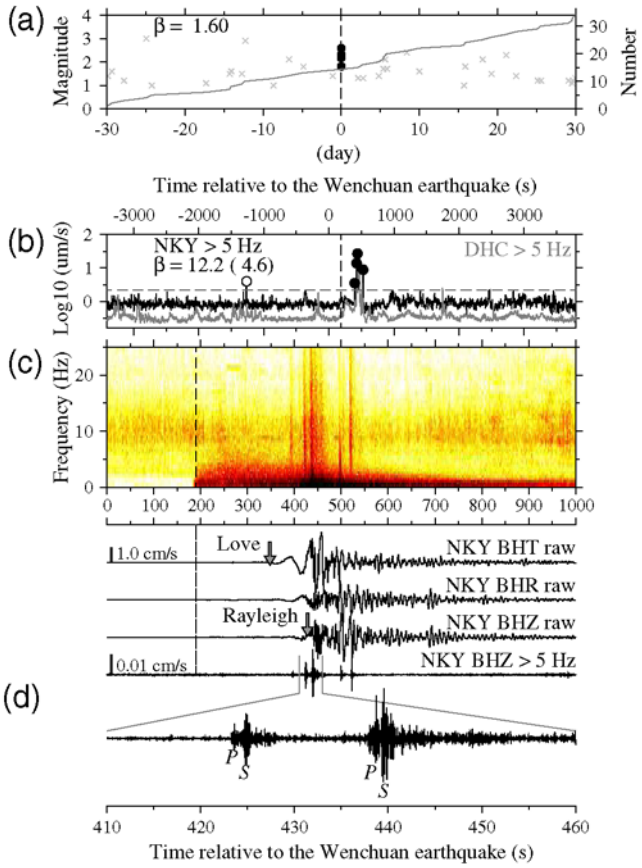

Figure 5. (a) Seismicity within 30 days of the Wenchuan mainshock and within 120 km of station BJ.NKY near Beijing. (b) The high-pass filtered envelope functions at station BJ.NKY (solid line) and nearby station BJ.DHC (gray line) within 1 hr of the P-wave arrival of the Wenchuan earthquake (vertical dashed line). (c) The spectrogram of the vertical-component seismogram recorded at station BJ.NKY. (d) Raw and high-pass filtered seismograms showing the teleseismic waves of the Wenchuan earthquake and locally generated seismic events, respectively. Other symbols and notations are the same as in Figure 3. The color version of this figure is available only in the electronic edition.

faults. The ß-values from the automatic and manual procedures are 4.6 and 12.2, respectively, and the β-values with longer time windows before the mainshock are larger than 2 (Fig. A1), further confirming that the triggered activity observed at BJ.NKY is statistically significant.

Stations CC.CHL, HE.CLI, and TJ.BAD are located near the aftershock zone of the 1976 M_w 7.6 Tangshan earthquake. Peng *et al.* (2010) found an M 2.0 event occurred near the southern segment of the Tangshan aftershock zone around 705 s after the origin time of the Wenchuan mainshock, and a few smaller events occurred within 1 hr after the mainshock. Here, we confirm that the triggered activity is statistically significant (i.e., the β-values from both the automatic and manual procedures are larger than 2).

We also find clear triggered activity at stations SX.SZZ, SX.SHZ, SX.PIG, and SX.DAX that are located within the

northern portion of the Shanxi graben (Zhang *et al.*, 1998), which is part of the rift systems surrounding the Ordos plateau. Figure 6 shows an example of seismic activity before and after the Wenchuan mainshock at stations SX.SZZ and SX.SHZ. We identified no events before and four events after the surface waves of the Wenchuan mainshock, and the associated β-values from the automatic and manual methods are 652.9 and 19.7, respectively. The large β-value from the automatic method is probably caused by the high-frequency energy during the slightly clipped surface waves. Because of this, we cannot rule out the possibility that additional earthquakes are triggered during the surface waves.

Finally, we find three stations (AH.LNA, JS.LYG, and JS.PX) in east China showing significant triggering activity. Among them, stations JS.LYG and AH.LNA are close to the Tanlu fault zone, the major boundary between the north China plain and the Jiaoliao and Hehuai plain fault blocks. Besides the activity triggered during and immediately after the surface waves, we also find two moderate-size events long after the mainshock. The first one was an M_L 3.8 event on 12 May 2008, 21:00 (6 hr and 32 min later), whose epicenter is 122-km away from JS.LYG. The second M_L 3.2 event occurred on 23 August 2008, and is 94-km away from JS.LYG. It is worth noting that the background seismicity in this region has been very low in the past 8 yr. A total of 25 $M_L > 3$ earthquakes occurred within 150 km of station JS.LYG since 2000, which corresponds to the probability of 0.82% for seeing an $M_L > 3$ earthquake in any given day. This value is a conservative estimate because the seismicity rate is extremely low immediately before and after the mainshock, based on the regional earthquake catalog. Hence, it is reasonably to assume that those two $M_L > 3$ earthquakes are likely triggered by the Wenchuan mainshock. In comparison, station JS.PX is ~164-km away from the epicenter of 1668 $M \sim$ 8.5 Tancheng earthquake, 185-km away from the epicenter of the 1 August 1937, $M \sim 7.0$ Heze earthquake and 156-km away from the epicenter of the 6 November 1983 M_s 6.0 Heze earthquake.

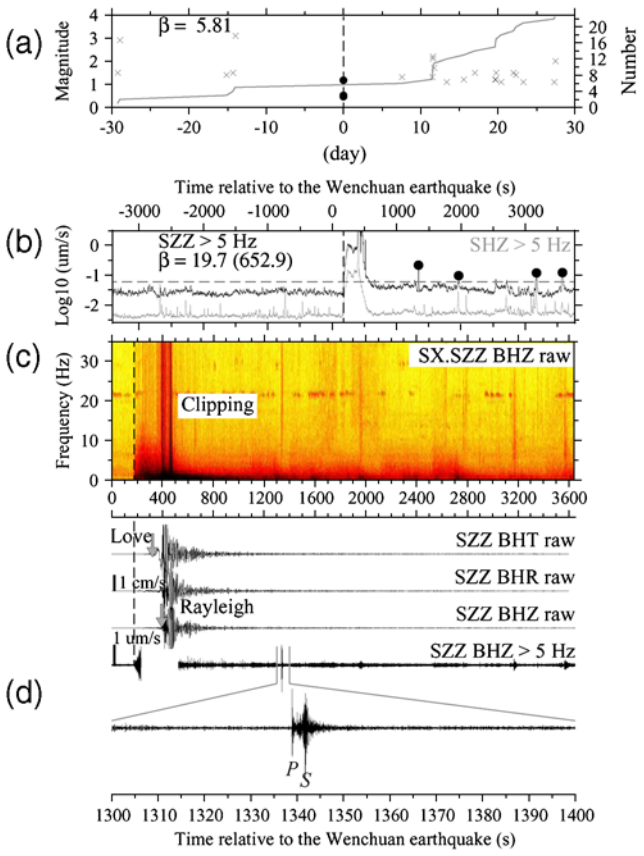

Figure 6. (a) Seismicity within 30 days of the Wenchuan mainshock and within 120 km of station SX.SZZ in the Shanxi province. (b) The high-pass filtered envelope functions at station SX.SZZ (solid line) and nearby station SX.SHZ (gray line) within 1 hr of the *P*-wave arrival of the Wenchuan earthquake (vertical dashed line). (c) The spectrogram of the vertical-component seismogram recorded at station SX.SZZ. (d) Raw and high-pass filtered seismograms showing the teleseismic waves of the Wenchuan earthquake and locally generated seismic events, respectively. Other symbols and notations are the same as in Figure 3. The color version of this figure is available only in the electronic edition.

Triggered Activity in Northeast China

The northeast China block includes the Heilongjiang, Jilin, and Liaoning provinces (Figs. 1 and 2e). The tectonic activity and background seismicity are much less active as compared with the three fault block regions described previously (Deng *et al.*, 2003). Although deep earthquakes are typical in this region, they are likely associated with the subduction of the Pacific plate underneath the Eurasian plate. In addition, the volcanic activity in the region is relatively strong. Many volcanoes, including Changbaishan, Wudalianchi, Jingbohu, and Longgang volcano clusters, are located in Jilin and Heilongjiang provinces.

We identify clearly triggered activity at two stations in northeast China. Station LN.LHT is very close to the northern extension of the Tanlu fault zone. We do not find any earthquake within 6 hr before the mainshock and one earthquake after the passage of the surface waves. The corresponding β-values with different pre-mainshock windows are larger than 2 (Ⓔsee Table S3, available in the electronic supplement to this paper). Station JL.BST is near the Longgang volcano, with the latest volcanic eruptions occurred about 1500–1600 yr ago (Fan *et al.*, 2002). The first earthquake signals occurred during the first few cycles of the surface waves and the other six appeared after 2800 s (Fig. 7). Although there are several earthquakes occurred before the Wenchuan mainshock, their amplitudes are smaller than those after the mainshock. The corresponding β-value from the hand-picked events with 1-hr time window is 3.6, and the β-values for other longer pre-mainshock time windows are also larger than 2. The value from the automatic procedure is much larger, mainly because of strong seismic energy in multiple frequency bands ranging 10–40 Hz (Fig. 7c).

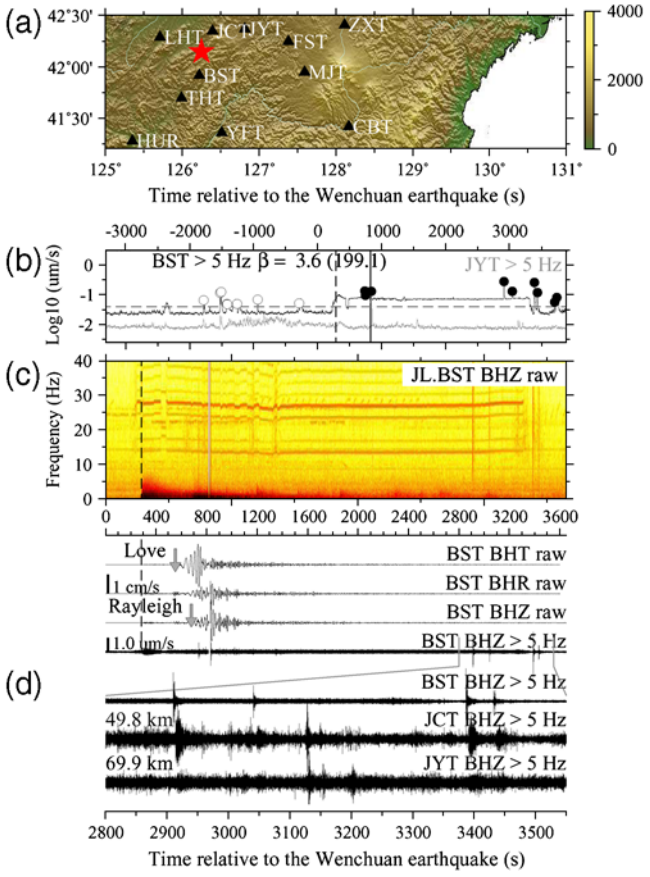

Figure 7. (a) The station distribution (black triangle) around the Longgang volcano (star) in the Jilin province. The background color shows the topography. (b) Seismicity within 30 days of the Wenchuan mainshock and within 120 km of station JL.BST near the Longgang volcano. (c) The high-pass filtered envelope functions at station JL.BST (solid line) and nearby station JL.JCT (gray line) within 1 hr of the *P*-wave arrival of the Wenchuan earthquake (vertical dashed line). (d) The spectrogram of the vertical-component seismogram recorded at station JL.BST. (e) Raw and high-pass filtered seismograms showing the teleseismic waves of the Wenchuan earthquake and locally generated seismic events. Other symbols and notations are the same as in Figure 3. The color version of this figure is available only in the electronic edition.

Such signals have similar characteristics of typical harmonic tremor observed at volcanic regions (e.g., Chouet, 1996). However, they are not recorded at nearby stations JL.THT, JL.JYT, JL.JCT, and JL.LHT, and probably not triggered by the Wenchuan earthquake because they occurred ~30 s before the arrivals of the *P* waves. It is worth noting that the Longgang volcano is the only volcano cluster in northeast China that responds to the Wenchuan earthquake.

Triggered Activity in South China

The south China block is a relatively stable block with little Quaternary tectonic deformation (Figs. 1 and 2f). The most active tectonic activity is concentrated at Longmen Shan–Xianshuhe–Red River fault system, which is the boundary between this block and the Tibetan plateau (e.g., Deng *et al.*, 2003; Liu *et al.*, 2007). In comparison, the Qinling-Dabie fault zone, which separates the north and south China blocks, is less active. Within the south China block, the tectonic deformation and background seismicity is minor as compared with other blocks in China. The only exception is the southeast coastal fault block, where several historical large earthquakes have occurred. These include the 29 December 1604 $M \sim 8.0$ Quanzhou earthquake in the Fujian province, the 13 February 1918 $M \sim 7.3$ Nan'ao earthquake in the Guangdong (Kanto) province, and the 13 July 1605 $M \sim 7.5$ earthquake in the Hainan Island.

We find a total of three stations that show clear triggered activity in the south China block. All of these stations are located along the southeast coast. The first station is ZJ.ZHS in the Zhejiang province (Fig. 8). The background seismicity in this region has been extremely low, with no $M_L > 4.5$ earthquake since 1 January 1970 and no $M > 5.5$ earthquake in recording history based on the China Historical Earthquake Catalog. Figure 8a shows that only one M_L 1.5 earthquake within 30 days of the Wenchuan event is reported in the regional earthquake catalog. Our visual inspection of the high-pass filtered seismograms identifies at least one event within 1 hr before and two events after the Wenchuan mainshock. The first event occurs at ~500 s in the first few cycles of the Love waves, and the second events occur at ~2300 s. Again, the seismometers were slightly off-scale during the large-amplitude Love and Rayleigh waves. Hence, we were unable to verify whether additional events occurred during these periods or not. The β-values from both automatic and manual procedures with 1-hr window are 30.9 and 6.2, respectively. However, we identify at least nine events between 4 and 2 hr before the mainshock, which causes the β-values to be less than 2 with pre-mainshock windows larger than 2 hr (Ⓔsee Tables S3 and S3, available in the electronic supplement to this paper). Hence, we cannot rule out the possibility that the observed activity after the mainshock is caused by random fluctuations of the background seismicity.

Triggered event is also identified at station FJ.FDQY (Fig. 9). There was no earthquake before and one event immediately after the Wenchuan mainshock. This event is large enough to be recorded by nearby stations FJ.SNQY, FJ.NDZW, FJ.ZHNZ, and ZJ.WEZ (Ⓔsee Fig. S2, available in the electronic supplement to this paper). The station FJ.FDQY is about 253 km from the epicenter of the 1604 $M \sim 8.0$ Quanzhou earthquake, which is the largest earthquake in the relatively stable south China block based on the historical catalog. The three flat lines between 1500 and 3000 s shown in Figure 9b were in the original data with unknown origins. This portion is included in the automatic beta calculation, but is excluded from the subsequent hand-picked analysis.

Figure 10 shows the seismic activity recorded at station HI.BSH in the Hainan Island. Again, this region is seismically quiet, and no earthquakes are reported in the regional

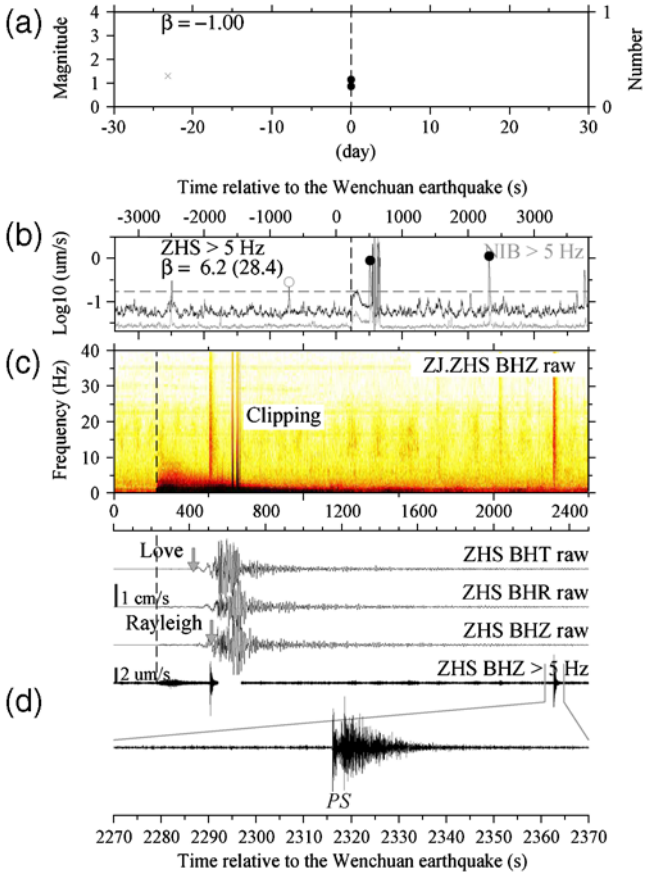

Figure 8. (a) Seismicity within 30 days of the Wenchuan mainshock and within 120 km of station ZJ.ZHS in the Zhejiang province. (b) The high-pass filtered envelope functions at station ZJ.ZHS (solid line) and nearby station ZJ.NIB (gray line) within 1 hr of the *P*-wave arrival of the Wenchuan earthquake (vertical dashed line). (c) The spectrogram of the vertical-component seismogram recorded at station ZJ.ZHS. (d) Raw and high-pass filtered seismograms showing the teleseismic waves of the Wenchuan earthquake and locally generated seismic events, respectively. Other symbols and notations are the same as in Figure 3. The color version of this figure is available only in the electronic edition.

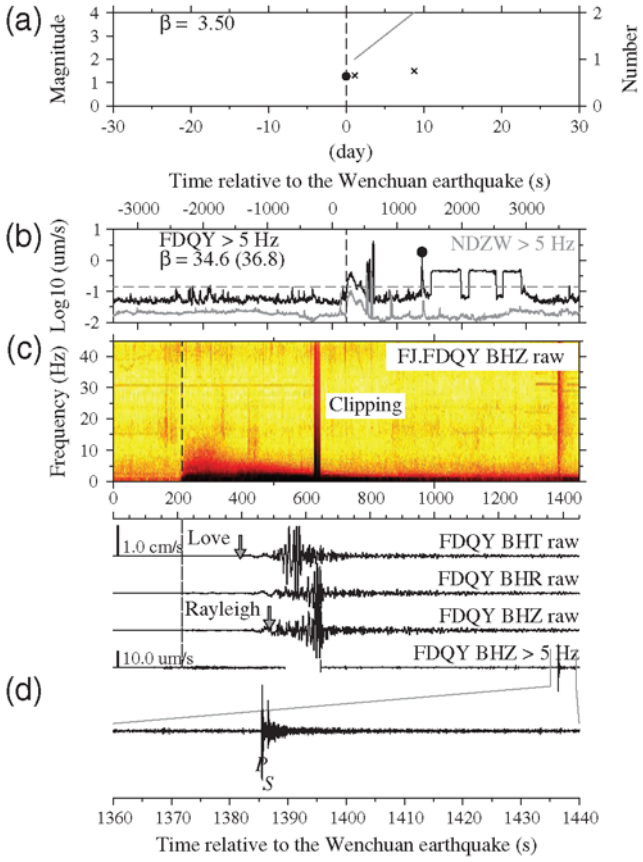

Figure 9. (a) Seismicity within 30 days of the Wenchuan mainshock and within 120 km of station FJ.FDQY in Fujian province. (b) The high-pass filtered envelope functions at station FJ.FDQY (solid line) and nearby station FJ.NDZW (gray line) within 1 hr of the *P*-wave arrival of the Wenchuan earthquake (vertical dashed line). (c) The spectrogram of the vertical-component seismogram recorded at station FJ.FDQY. (d) Raw and high-pass filtered seismograms showing the teleseismic waves of the Wenchuan earthquake and locally generated seismic events, respectively. Other symbols and notations are the same as in Figure 3. The color version of this figure is available only in the electronic edition.

earthquake catalog within 30 days before and after mainshock. From the high-pass filtered envelopes, we find no earthquakes within 1 hr with *S*-*P* times less than 15 s before the Wenchuan mainshock. Similar to the station ZJ.ZHS, the seismograms are slightly clipped during the large-amplitude surface waves. We only identify one event at ~2900 s after the mainshock, long after the seismograms went back onscale. The automatic and manual β-values are large, which may be caused by the fact that no earthquake is identified before the mainshock and that there is a slight clipping during the surface waves. However, we identified an event with larger amplitudes between 2 to 3 hr before the mainshock, which causes the manual β-values to be less than 2 for longer time windows. Similar to station ZJ.ZHS, we suggest that the observed triggering effect at this station is less significant as compared other stations.

Summary of Observations

In summary, of the 271 stations we have examined, we found 17 stations with statistically significant triggering activity (i.e., with the automatic and manual β-statistic values > 2). Among them, 11 stations are located in the north China block, which is tectonically active with many large earthquakes in the past. Most of these stations are located near active faults that have been ruptured in historic times. In the seismically active northwest China, station QH.QIL and other nearby stations close to the Haiyuan fault zone recorded clear local seismic signals triggered by the Wenchuan earthquake (Fig. 3 and Ⓔ Fig. S1, available in the electronic supplement to this paper). In the north China block, station BJ.NKY is very close to the Babaoshan and Huangzhuang–Gaoliying faults, a major boundary between the Taihang Mountain to the west and the Bohai Bay Basin to the east.

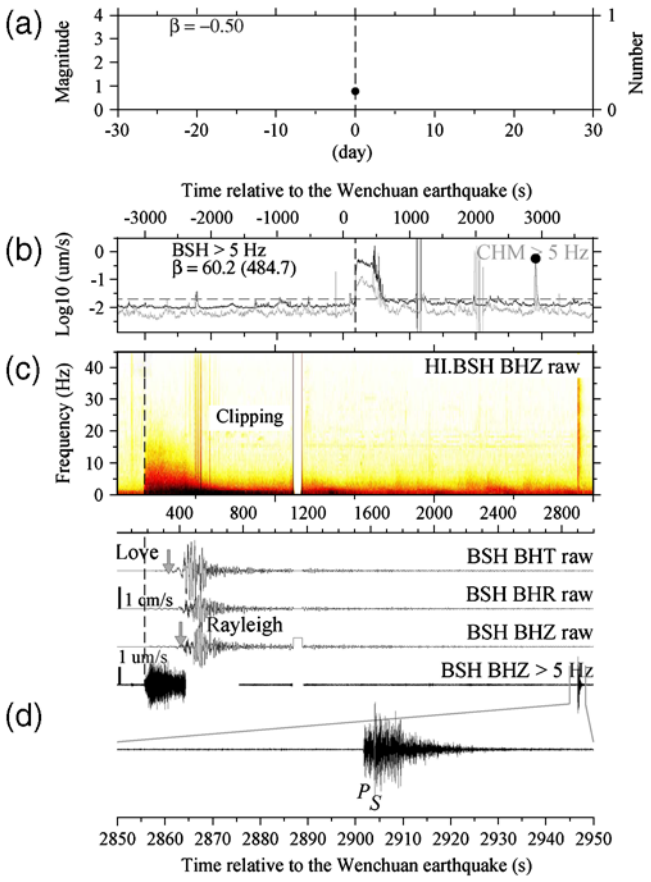

Figure 10. (a) Seismicity within 30 days of the Wenchuan mainshock and within 120 km of station HI.BSH in Hainan. No earthquake is listed in the catalog during the space-time window. (b) The high-pass filtered envelope functions at station HI.BSH (solid line) and nearby station HI.CHM (gray line) within 1 hr of the *P*-wave arrival of the Wenchuan earthquake (vertical dashed line). (c) The spectrogram of the vertical-component seismogram recorded at station HI.BSH. (d) Raw and high-pass filtered seismograms showing the teleseismic waves of the Wenchuan earthquake and locally generated seismic events, respectively. Other symbols and notations are the same as in Figure 3. The color version of this figure is available only in the electronic edition.

Stations CC.CHL, HE.CLI, and TJ.BAD are located near the rupture zone of the 1976 M_w 7.6 Tangshan earthquake. Stations SX.SZZ, SX.SHZ, SX.PIG, SX.DAX, and SX.DOS that are located within the Shanxi graben, a rift system surrounding the Ordos plateau. Stations JS.LYG and AH.LNA are close to the Tanlu fault zone, the major boundary between the north China plain and the Jiaoliao and Hehuai plain fault blocks. In the northeast China block, the only two stations with seismic activity triggered by the Wenchuan earthquake are LH.LHT close to the Tanlu fault zone and JL.BST that is located very close to the Longgang Volcano in the Jilin province. In the south China block, only three stations along the relatively active southeast coast fault block show clearly triggered activity.

To further quantify the observation, we plot the azimuths of all 271 stations relative to the Wenchuan epicenter against their distances to major faults (Fig. 11). Here, we use the major block-boundary faults as described in Deng *et al.* (2003). It is possible that some stations are close to other active faults that do not belong to the major block-boundary faults. Hence, the distance estimated here is likely a higher bound. Nevertheless, as mentioned before, a general observation is that most stations that show clear triggering are in the rupture propagation direction in north China. In addition, except for stations FJ.FDQY, HI.BST, and JS.PX, other stations showing clear triggering are within 100 km of the major faults. Because we use *S-P* times of 15 s as a criterion to select local events, it is reasonable to assume that most of the triggered activity likely occurs close or on those major faults.

Distribution of the Peak Dynamic Stresses

Many studies have shown that dynamic stress from the passing surface waves plays an important role in controlling the triggering activity in different locations (e.g., Hill *et al.*, 1993; Prejean *et al.*, 2004; Brodsky and Prejean, 2005; Gomberg and Johnson, 2005; Peng *et al.*, 2009; Rubinstein *et al.*, 2009; van der Elst and Brodsky, 2010). Assuming plane wave propagation for teleseismic waves, the peak dynamic stress σ_d is proportional to $G \times \dot{u}/v_s$ (Jaeger and Cook, 1979), where G is the shear modulus, $\dot{u}$ is the peak ground velocity (PGV), and v_s is the phase velocity. The PGVs measured from the instrument corrected vertical

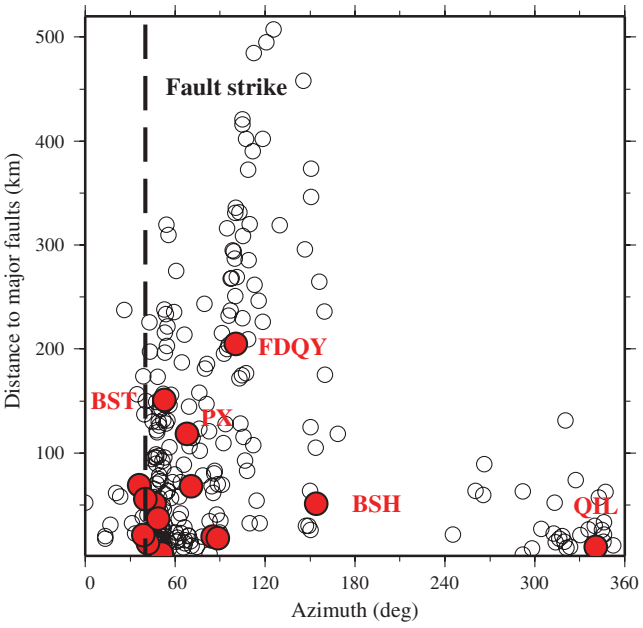

Figure 11. The azimuths of all 271 stations relative to the Wenchuan epicenter versus the distances to major block-boundary faults (Deng *et al.*, 2003). The large circles mark the 17 stations that show triggering with selected station names marked. The vertical dashed line marks the fault strike of the Beichuan fault that ruptured during the Wenchuan earthquake (Xu *et al.*, 2009). The color version of this figure is available only in the electronic edition.

seismograms are in the range of ~0.3–1.8 cm/s. Using a nominal G-value of 35 GPa and $v_s = 3.5$ km/s for the Rayleigh waves, we estimate the dynamic stress to be in the range of ~0.03–0.18 MPa (Fig. 12). We note that many stations with slight clipping during the large-amplitude surface waves are included in the analysis. Hence, the PGVs and the corresponding dynamic stresses are lower-bound estimates for those stations.

Discussion

In this study, we conducted an extensive search of remotely triggered seismicity in continental China following the 2008 M_w 7.9 Wenchuan earthquake. Our work is, to our own knowledge, the first systematic and complete survey of dynamic triggering in an intraplate region based on modern broadband instrumental recordings. Our observations are inevitably colored by the uneven station distributions (for example, comparing the station density in north/south China blocks and Tibetan and Xinjiang blocks in the west). In addition, the seismic data recorded by many stations within 1000 km of the mainshock epicenter are severely clipped during the large surface waves, which prevent us from studying dynamic triggering in the regional distances. Nevertheless, we attempt to provide some insights on the necessary conditions of dynamic triggering in intraplate regions based on such uneven samplings.

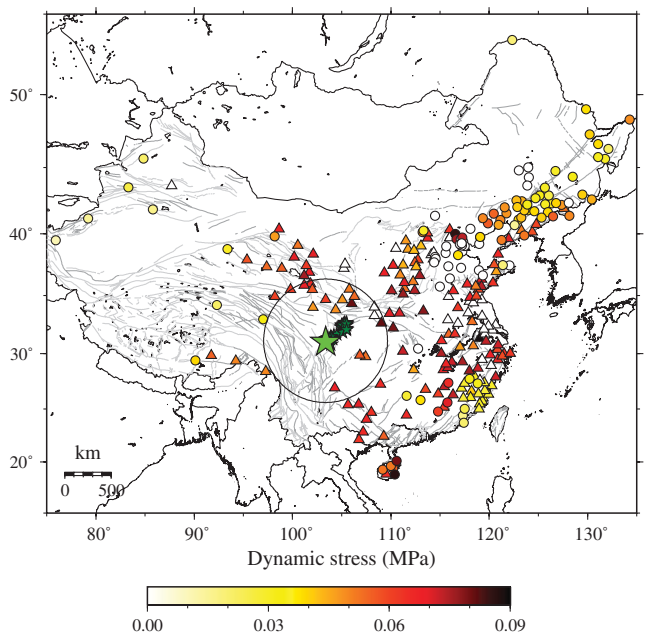

Figure 12. Distribution of the dynamic stresses estimated from the peak ground velocities in the vertical-component seismograms. The triangles mark stations with slight clippings during the surface waves of the Wenchuan earthquake, and the circles mark those recorded onscale. The large circle corresponds to the 600 km from the epicenter of the Wenchuan mainshock (large solid star). The color version of this figure is available only in the electronic edition.

As summarized before, it appears that the proximity to active faults (or aftershock zones of historic earthquakes) and rupture propagation directions of the mainshock are two conditions that would favor remote triggering in intraplate regions (Fig. 11). The most significant triggering was found in north China with many active faults and historic seismic activity, and is in the rupture propagation direction of the Wenchuan earthquake. In comparison, we only find one site with clear triggerng near the Haiyuan fault in the tectonically active Tibetan and Xinjiang blocks, which are not in the rupture propagation directions. Another negative example is station XJ.KSH (Fig. 4) near the border of the Tianshan Mountain and Tarim basin. Despite the close distance to active faults and elevated background seismicity, no triggered activity is found at this station, probably because of the relatively low dynamic stresses (~0.02 MPa) in this area. In relatively stable south China block, the dynamic stresses are in the intermediate range (0.03–0.08 MPa). No triggering is identified for most stations within the south China block, although the corresponding dynamic stresses are larger than those three sites with clear triggering along the relatively active southeast coast fault block.

Our results are generally consistent with previous studies of dynamic triggering in intraplate regions. In particular, Hough *et al.* (2003) found that remotely triggered earthquakes in the central and eastern U.S. following the 1811–1812 New Madrid earthquake sequences and the 1886 Charleston earthquake tend to occur at sites known to be seismically active during historic times. A recent survey of coseismic strain steps from the borehole strain monitoring network of China following the 2001 M_w 7.8 Kunlun earthquake have found that large strain steps were observed at stations only in the tectonically active northeastern China but not in the relatively inactive southeastern China (Qiu and Shi, 2004). They inferred that the coseismic strain steps are caused by locally triggered earthquakes, which are more likely observed in tectonically active regions. These results suggest that regions with active faults (some may have ruptured previously with ongoing aftershock activity) in intraplate regions are more susceptible to dynamic triggering, most likely because these regions represent zones of weakness or stress concentrations, and hence contain nucleation points more frequently closer to failure (e.g., Hill *et al.*, 1993; Hough *et al.*, 2003; Hill and Prejean, 2007; Hough, 2007; Savage and Marone, 2008).

In addition, the influence of the rupture directivity effect on the distribution of dynamic triggering has been observed for many cases from the near field (Kilb *et al.*, 2002; Gomberg *et al.*, 2003) to long-range distances (Gomberg *et al.*, 2001; Gomberg *et al.*, 2004). Here, we found that the rupture propagation directions, or more specifically, the peak ground velocities of the surface waves also contribute to determine the regions that show triggered activity. However, it is worth pointing that these two conditions are neither necessary nor sufficient thresholds for dynamic triggering. For example, many stations in the northeast direction (the rupture propagation directions) within ~1200 km of

the mainshock epicenter are also very close to the Weihe-Shanxi graben. Although these regions are seismically quiet at present, many historical earthquakes occurred in the past 800 yr (e.g., Li, Liu, and Stein, 2009). However, we did not identify any clear triggered activity at these locations. One possible reason is that the seismic signals at these stations are clipped during the large surface waves, hence preventing us from identifying locally triggered seismic signals during these time periods. In addition, the intensive aftershock activity from the mainshock rupture zone could also hide seismic signals generated by small local earthquakes. Another possible explanation could be that if the threshold of remotely triggered seismicity is frequency dependent (e.g., Brodsky and Prejean, 2005; Guilhem *et al.*, 2010), then only long-period surface waves at larger distances have higher potential of triggering earthquakes. A careful examination of onscale recording of strong ground motion recordings (e.g., Li, Zhou, *et al.*, 2009) could help to verify whether earthquakes are triggered locally at these regions.

Because the background seismicity could vary in space and time, the observed seismicity change associated with the Wenchuan mainshock could also be contaminated by a random fluctuation of the seismicity rate. In this study, we evaluated a longer time window before the mainshock and compute the corresponding β-value. We found that at stations SX.DAX, ZJ.ZHS, and HI.BSH, sometimes the β-values with longer time windows (up to 6 hr) before the mainshock are less than 2 (Ⓔsee Table S3, available in the electronic supplement to this paper). Because we use the same time window (1 hr) after the mainshock to compute the β-values, the variation in the β-value is caused by the fluctuation of background seismicity before the mainshock. Because of this, we suggest that the observed triggering at these stations could have a higher potential of being contaminated by random fluctuations of background seismicity than at other stations.

As summarized in the introduction, many physical models have been proposed to explain remotely triggered seismicity, which can be classified into two categories (e.g., Hill and Prejean, 2007): triggering through frictional failure and through excitation of crustal fluids (either hydrous or magmatic). Because of a lack a thorough knowledge of the triggering wavefield, accurate locations of the triggered earthquakes, and ambient conditions at each site, we cannot provide a better constraint on the physical models for the triggering processes in the intraplate region at this stage. Here, we attempt to make some inferences on the physical models based on the available information and observations.

First, we note that except for one station near the Longgang volcano in the Jilin province, most stations occur in tectonic regions away from active geothermal or volcanic regions. Hence, it is less likely that the fluid-based models would apply to these regions. In addition, at stations BJ.NKY and ZJ.ZHS, the first triggered earthquake coincides with the first few cycles of the Love waves (Figs. 5 and 8). Recent studies on triggered earthquakes and nonvolcanic tremor have shown that Rayleigh wave triggering could be explained by both the frictional failure model and the fluid-based model (Miyazawa and Brodsky, 2008). On the other hand, triggering by the Love waves could only be explained by the frictional failure model, because of the inability of the Love wave particle motion to move fluids (Rubinstein *et al.*, 2007; Hill, 2008; Peng *et al.*, 2008; Peng and Chao, 2008; Peng *et al.*, 2009; Rubinstein *et al.*, 2009). Hence, at least in these two regions, it appears that the frictional failure model provides a better explanation for the observed triggering activity. However, at the rest of the stations, the first triggering event occurs after the passage of the large-amplitude surface waves. Again, at least part of the reason could be caused by clipping of seismograms during the large-amplitude surface waves, which may prevent triggered activity from being observed during that period (e.g., Figs. 3, 6, 8, 9). In addition, Hill and Prejean (2007) suggested that in many cases the onset of triggering earthquakes begins at some times after the passage of surface waves. Finally, we only examined the continuous recordings within 1 hr after the Wenchuan mainshock, and use the regional earthquake catalog for the rest 30-day time period before and after the mainshock. Because of this, we may omit delayed onsets of triggered seismicity, which are more likely caused by excitations of fluids, or aseismic creep (e.g., Johnston *et al.*, 2004; Prejean *et al.*, 2004). Systematic studies of selected sites with clear triggered activity (e.g., BJ.NKY) and additional geophysical measurements are needed to better constrain the physical modes of remote triggering in intraplate regions. This will be done in a follow-up work.

Data and Resources

The continuous waveform data analyzed in this study were requested from the China Earthquake Data Center. The historical Chinese earthquake catalog from 1831 B.C. to 1969 A.D. can be downloaded from http://data.earthquake.cn/data/index.jsp?id=31&number=1 (last accessed 15 March 2010; in Chinese; no login required). The modern Chinese earthquake catalog since 1970 can be downloaded from http://data.earthquake.cn/data/index.jsp?no=11&number=4 (last accessed 15 March 2010; in Chinese; no login required).

Acknowledgments

We thank the China Earthquake Data Center for providing the seismic data used in this study. T. J. is supported by the National Natural Science Foundation of China (grant 40674096) and the China Young Faculty Scholarship from the China Scholarship Council. Z. P. is supported by the National Science Foundation (grants EAR-0809834 and EAR-0956051) and Georgia Tech College of Science Faculty Research Development Grant. W. W. and Q. F. C. are supported by Special Scientific Research Projects on Earthquake (Grant 200708008). The manuscript benefited from valuable comments by David Hill, Peng Zhao, associate editor Zheng-Kang Shen, reviewer Honn Kao, and an anonymous reviewer.

References

Anderson, J. G., J. N. Brune, J. N. Louie, Y. Zeng, M. Savage, G. Yu, Q. Chen, and D. dePolo (1994). Seismicity in the western Great Basin apparently triggered by the Landers, California, earthquake, 28 June 1992, *Bull. Seismol. Soc. Am.* **84,** 844–854.

Avouac, J. P. (2008). Dynamic processes in extensional and compressional settings—mountain building: From earthquakes to geological deformation, *Treatise on Geophysics* **6,** Elsevier, Amsterdam, 377–439.

Brodsky, E. E., and S. G. Prejean (2005). New constraints on mechanisms of remotely triggered seismicity at Long Valley Caldera, *J. Geophys. Res.* **110,** B04302, 1–14.

Brodsky, E. E., V. Karakostas, and H. Kanamori (2000). A new observation of dynamically triggered regional seismicity: Earthquakes in Greece following the August, 1999 Izmit, Turkey earthquake, *Geophys. Res. Lett.* **27,** 2741–2744.

Brodsky, E. E., E. Roeloffs, D. Woodcock, I. Gall, and M. Manga (2003). A mechanism for sustained groundwater pressure changes induced by distant earthquakes, *J. Geophys. Res.* **108,** 2390, doi 10.1029/2002JB002321.

Brodsky, E. E., B. Sturtevant, and H. Kanamori (1998). Volcanoes, earthquakes and rectified diffusion, *J. Geophys. Res.* **103,** 23,827–23,838.

Burchfiel, B. C., L. H. Royden, R. D. van der Hilst, B. H. Hager, Z. Chen, R. W. King, C. Li, J. Lüc, H. Yao, and E. Kirby (2008). A geological and geophysical context for the Wenchuan earthquake of 12 May 2008, Sichuan, People's Republic of China, *GSA Today* **18,** 4–11.

Cavalié, O., C. Lasserre, M.-P. Doin, G. Peltzer, J. Sun, X. Xu, and Z.-K. Shen (2008). Measurement of interseismic strain across the Haiyuan fault (Gansu, China), by InSAR, *Earth Planet. Sci. Lett.* **275,** 246–257.

Chen, L., T. Wang, L. Zhao, and T. Y. Zheng (2008). Distinct lateral variation of lithospheric thickness in the northeastern north China Craton, *Earth Planet. Sci. Lett.* **267,** 56–68.

Chouet, B. A. (1996). Long-period volcano seismicity: Its source and use in eruption forecasting, *Nature* **380,** 309–316.

Deng, Q., P. Zhang, Y. Ran, X. Yang, W. Min, and Q. Chu (2003). Basic characteristics of active tectonics of China, *Sci. China Earth Sci.* **46,** 356–372.

Fan, Q., J. Sui, R. Liu, H. Wei, D. Li, Q. Sun, and N. Li (2002). Periods of Quarternary volcanic activity in Longgang area, Jilin province, *Acta Petrologica Sinica* **18,** 495–500.

Gomberg, J., and P. Johnson (2005). Dynamic triggering of earthquakes, *Nature* **437,** 830.

Gomberg, J., M. L. Blanpied, and N. M. Beeler (1997). Transient triggering of near and distant earthquakes, *Bull. Seismol. Soc. Am.* **87,** 294–309.

Gomberg, J., P. Bodin, K. Larson, and H. Dragert (2004). Earthquakes nucleated by transient deformations caused by the *M* 7.9 Denali, Alaska, earthquake, *Nature* **427,** 621–624.

Gomberg, J., P. Bodin, and P. A. Reasenberg (2003). Observing earthquakes triggered in the near field by dynamic deformations, *Bull. Seismol. Soc. Am.* **93,** 118–138.

Gomberg, J., P. A. Reasenberg, P. Bodin, and R. Harris (2001). Earthquakes triggering by seismic waves following the Lander and Hector Mine earthquakes, *Nature* **411,** 462–465.

Gomberg, J., P. Reasenberg, M. Cocco, and M. E. Bardinelli (2005). A frictional population model of seismicity rate change, *J. Geophys. Res.* **110,** B05S03, 1–10.

Gomberg, J., J. L. Rubinstein, Z. Peng, K. C. Creager, J. E. Vidale, and P. Bodin (2008). Widespread triggering of non-volcanic tremor in California, *Science* **319,** 173, doi 10.1126/science.1149164.

Guilhem, A., Z. Peng, and R. M. Nadeau (2010). High-frequency identification of non-volcanic tremor along the San Andreas fault triggered by regional earthquakes, *Geophys. Res. Lett.* doi 10.1029/2010GL044660, in press.

Gutenberg, R., and C. F. Richter (1944). Frequency of earthquakes in California, *Bull. Seismol. Soc. Am.* **34,** 185–188.

Harrington, R. M., and E. E. Brodsky (2006). The absence of remotely triggered seismicity in Japan, *Bull. Seismol. Soc. Am.* **96,** 871–878.

Hill, D. P. (2008). Dynamic stresses, coulomb failure, and remote triggering, *Bull. Seismol. Soc. Am.* **98,** 66–92.

Hill, D. P., and S. G. Prejean (2007). Dynamic triggering, in *Earthquake Seismology Treatise on Geophysics*, H. Kanamori (Editor), Elsevier, Amsterdam.

Hill, D. P., F. Pollitz, and C. Newhall (2002). Earthquake-volcano interactions, *Phys. Today* **55,** 41–47.

Hill, D. P., P. A. Reasenberg, A. Michael, W. J. Arabaz, G. Beroza, D. Brumbaugh, J. N. Brune, R. Castro, S. Davis, D. dePolo, W. L. Ellsworth, J. Gomberg, S. Harmsen, L. House, S. M. Jackson, M. J. S. Johnston, L. Jones, R. Keller, S. Malone, L. Munguia, S. Nava, J. C. Pechmann, A. Sanford, R. W. Simpson, R. B. Smith, M. Stark, M. Stickney, A. Vidal, S. Walter, V. Wong, and J. Zollweg (1993). Seismicity remotely triggered by the magnitude 7.3 Landers, California, earthquake, *Science* **260,** 1617–1623.

Hough, S. E. (2005). Remotely triggered earthquakes following moderate mainshocks (or, why California is not falling into the ocean), *Seismol. Res. Lett.* **76,** no. 1, 58–66.

Hough, S. E. (2007). Remotely triggered earthquakes following moderate main shocks, S. Stein and S. Mazzotti (Editors), Geol. Soc Am. Special Papers, Boulder, Colorado, 73–86.

Hough, S. E., and H. Kanamori (2002). Source properties of earthquakes near the Salton Sea triggered by the 16 October, 1999 *M* 7.1 Hector Mine earthquake, *Bull. Seismol. Soc. Am.* **92,** 1281–1289.

Hough, S. E., L. Seeber, and J. G. Armbruster (2003). Intraplate triggered earthquakes; observations and interpretation, *Bull. Seismol. Soc. Am.* **93,** 2212–2221.

Husen, S., S. Wiemer, and R. B. Smith (2004). Remotely triggered seismicity in the Yellowstone National Park region by the 2002 M_w 7.9 Denali fault earthquake, Alaska, *Bull. Seismol. Soc. Am.* **94,** S317–S331.

Husker, A., and E. E. Brodsky (2004). Dynamically triggered seismicity in Idaho and western Montana: The necessary geology, *Bull. Seismol. Soc. Am.* **94,** S310–S316.

Jaeger, J. C., and N. G. W. Cook (1979). *Fundamentals of rock mechanics*, Third Ed., Chapman and Hall, New York.

Johnson, P. A., and X. Jia (2005). Nonlinear dynamics, granular media and dynamic earthquake triggering, *Nature* **437,** 871–864.

Johnston, M. J. S., S. G. Prejean, and D. P. Hill (2004). Triggered deformation and seismic activity under Mammoth Mountain in Long Valley Caldera by the 3 November 2002 M_w 7.9 Denali Fault earthquake, *Bull. Seismol. Soc. Am.* **94,** S360–S369.

Kennett, B. L. N., and E. R. Engdahl (1991). Traveltimes for global earthquake location and phase identification, *Geophys J. Int.* **105,** 429–465.

Kilb, D., J. Gomberg, and P. Bodin (2002). Aftershock triggering by complete Coulomb stress changes, *J. Geophys. Res.* **107,** no. B4, 2060, doi 10.1029/2001JB000202.

Li, Q., M. Liu, and S. Stein (2009). Spatial-temporal complexity of continental intraplate seismicity: Insights from geodynamic modeling and implications for seismic hazard estimation, *Bull. Seismol. Soc. Am.* **99,** 52–60.

Li, X., Z. Zhou, M. Huang, R. Wen, H. Yu, D. Lu, Y. Zhou, and J. Cui (2009). Preliminary analysis of strong-motion recordings from the magnitude 8.0 Wenchuan, China, Earthquake of 12 May 2008, *Seismol. Res. Lett.* **79,** 844–854.

Linde, A. T., M. Gladwin, M. Johnston, R. Gwyther, and R. Bilham (1996). A slow earthquake sequence on the San Andreas fault, *Nature* **383,** 65–68.

Liu, M., Y. Yang, Z.-K. Shen, S. Wang, M. Wang, and Y. Wan (2007). Active tectonics and intracontinental earthquakes in China: The kinematics and geodynamics, in *Continental Intraplate Earthquakes: Science, Hazard, and Policy Issues*, S. Stein and S. Mazzotti (Editors), Geol. Soc Am. Special Papers, Boulder, Colorado, 299–318, doi 210.1130/2007.2425 (**19**).

Matthews, M. V., and P. A. Reasenberg (1988). Statistical methods for investigating quiescence and other temporal seismicity patterns, *Pure Appl. Geophys.* **126,** 357–372.

Miyazawa, M., and J. Mori (2005). Detection of triggered deep low-frequency events from the 2003 Tokachi-oki earthquake, *Geophys. Res. Lett.* **32,** L10307, doi 10.1029/2005GL022539.

Miyazawa, M., and J. Mori (2006). Evidence suggesting fluid flow beneath Japan due to periodic seismic triggering from the 2004 Sumatra-Andaman earthquake, *Geophys. Res. Lett.* **33,** L05303, doi 10.1029/2005GL025087.

Miyazawa, M., and E. E. Brodsky (2008). Deep low-frequency tremor that correlates with passing surface waves, *J. Geophys. Res.* **113,** B01307, doi 10.1029/2006JB004890.

Miyazawa, M., E. E. Brodsky, and J. Mori (2008). Learning from dynamic triggering of low-frequency tremor in subduction zones, *Earth Planets Space* **60,** e17–e20.

Omori, F. (1894). On the aftershocks of earthquakes, *J. Coll. Sci. Imp. Univ. Tokyo* **7,** 111–200.

Pankow, K. L., W. J. Arabaz, J. C. Pechmann, and S. J. Nava (2004). Triggered seismicity in Utah from the 3 November 2002 Denali fault earthquake, *Bull. Seismol. Soc. Am.* **94,** S332–S347.

Peng, Z., and K. Chao (2008). Non-volcanic tremor beneath the Central Range in Taiwan triggered by the 2001 M_w 7.8 Kunlun earthquake, *Geophys. J. Int.* **175,** 825–829.

Peng, Z., J. E. Vidale, K. C. Creager, J. L. Rubinstein, J. Gomberg, and P. Bodin (2008). Strong tremor near Parkfield, CA excited by the 2002 Denali Fault earthquake, *Geophys. Res. Lett.* **35,** L23305, doi 10.1029/2008GL036080.

Peng, Z., J. E. Vidale, M. Ishii, and A. Helmstetter (2007). Seismicity rate immediately before and after main shock rupture from high-frequency waveforms in Japan, *J. Geophys. Res.* **112,** B03306, doi 10.1029/2006JB004386.

Peng, Z., J. E. Vidale, A. Wech, R. M. Nadeau, and K. C. Creager (2009). Remote triggering of tremor along the San Andreas fault in central California, *J. Geophys. Res.* **114,** B00A06, doi 10.1029/2008JB006049.

Peng, Z., W. Wang, Q.-F. Chen, and T. Jiang (2010). Remotely triggered seismicity in north China following the 2008 M_w 7.9 Wenchuan earthquake, *Earth Planets Space*, in press.

Perfettini, H., J. Schmittbuhl, and A. Cochard (2003). Shear and normal load perturbations on a two-dimensional continuous fault: 2 dynamic triggering, *J. Geophys. Res.* **108,** 2409, doi 10.1029/2002JB001805.

Prejean, S. G., D. P. Hill, E. E. Brodsky, S. E. Hough, M. H. S. Johnston, S. D. Malone, D. H. Oppenheimer, A. M. Pitt, and K. B. Richards-Dinger (2004). Remotely triggered seismicity on the United States west coast following the *M* 7.9 Denali fault earthquake, *Bull. Seismol. Soc. Am.* **94,** S348–S359.

Qiu, Z., and Y. Shi (2004). Application of observed strain steps to the study of remote earthquake stress triggering, *Acta Seismologica Sinica* **17,** 534–541.

Reasenberg, P. A., and R. W. Simpson (1992). Response of regional seismicity to the static stress change produced by the Loma Prieta earthquake, *Science* **255,** 1687–1690.

Rubinstein, J. L., J. Gomberg, J. E. Vidale, A. G. Wech, H. Kao, K. C. Creager, and G. Rogers (2009). Dynamic triggering of non-volcanic tremor, ETS, and earthquakes on Vancouver Island, *J. Geophys. Res.* **114,** B00A01, doi 10.1029/2008JB005875.

Rubinstein, J. L., J. E. Vidale, J. Gomberg, P. Bodin, K. C. Creager, and S. D. Malone (2007). Non-volcanic tremor driven by large transient shear stresses, *Nature* **448,** 579–582.

Savage, H., and C. Marone (2008). The potential for earthquake triggering from transient deformations, *J. Geophys. Res.* **113,** B05302, doi 10.1029/2007JB005277.

Shelly, D. R., G. C. Beroza, and S. Ide (2007). Non-volcanic tremor and low-frequency earthquake swarms, *Nature* **446,** 305–307.

Stein, S. (2007). Approaches to continental intraplate earthquake issues, in *Continental intraplate earthquakes: Science, hazard, and policy issues*, S. Stein and S. Mazzotti (Editors), Geol. Soc Am. Special Paper 425, Boulder, Colorado, 1–16, doi 10.1130/2007.2425 (**01**).

Utsu, T. (2002). A list of deadly earthquakes in the World: 1500–2000, in W. K. Lee, H. Kanamori, P. C. Jennings, and C. Kisslinger (Editors), *International handbook of earthquake engineering and seismology*, Academic Press, Amsterdam, 691–717.

Utsu, T., Y. Ogata, and R. S. Matsu'ura (1995). The centenary of the Omori formula for a decay law of aftershock activity, *J. Phys. Earth* **43,** 1–33.

van der Elst, N. J., and E. E. Brodsky (2010). Connecting nearfield and farfield earthquake triggering to dynamic strain, *J. Geophys. Res.* **115,** B07311, doi 10.1029/2009JB006681.

Velasco, A. A., S. Hernandez, T. Parsons, and K. Pankow (2008). Global ubiquity of dynamic earthquake triggering, *Nature Geosci.* **1,** 375–379.

West, M., J. J. Sanchez, and S. R. McNutt (2005). Periodically triggered seismicity at Mount Wrangell, Alaska, after the Sumatra earthquake, *Science* **308,** 1144–1146.

Xu, X., X. Wen, G. Yu, G. Chen, Y. Klinger, J. Hubbard, and J. Shaw (2009). Coseismic reverse- and oblique-slip surface faulting generated by the 2008 M_w 7.9 Wenchuan earthquake, *China; Geology* **37,** 515–518.

Zhang, P., Q. Deng, G. Zhang, J. Ma, W. Gan, W. Min, F. Mao, and Q. Wang (2003). Active tectonic blocks and strong earthquakes in the continental of China, *Sci. China Earth Sci.* **46,** (Supplement S) 13–24.

Zhang, Y.-Q., J. L. Mercier, and P. Vergély (1998). Extension in the graben systems around the Ordos (China), and its contribution to the extrusion tectonics of south China with respect to Gobi-Mongolia, *Tectonophysics* **285,** 41–75.

Appendix

β-Statistic

A widely used procedure to test for the significance of seismicity rate changes associated with earthquake triggering is to compute the β-statistic (e.g., Matthews and Reasonberg, 1988; Reasenberg and Simpson, 1992; Hill and Prejean, 2007). The β-statistic is defined by

$$\beta(n_a, n_b; t_a, t_b) = \frac{n_a - E(n_a)}{\mathrm{Var}(n_a)}, \qquad \text{(A1)}$$

where n_b and n_a are the number of earthquakes observed before and after the mainshock, t_b and t_a are the time duration before and after the mainshock, respectively. The $E(n_a)$ is the expected number of earthquakes during t_a, and $\mathrm{var}(n_a)$ is the variance. Depending on the different assumption of the process for the background seismicity, the expected number and the variance are slightly different.

For a Poisson process (Hill and Prejean, 2007),

$$E(n_a) = \mathrm{var}(n_a) = n_b(t_a/t_b). \qquad \text{(A2)}$$

For a Binomial process (e.g., Gomberg *et al.*, 2001; Kilb *et al.*, 2002; Pankow *et al.*, 2004; Hough, 2005),

$$E(n_a) = np = t_a(n_b/t_b), \quad \text{and}$$
$$\mathrm{var}(n_a) = npq = t_a(n_b/t_b)(1 - n_b/t_b), \qquad \text{(A3)}$$

where $p = n_b/t_b$ is the probability of earthquake occurrence (or earthquake rate) before the mainshock. When p is small

enough, the Poisson process is a good approximation of the binomial process, and both formulas give similar results. Results with $|\beta| > 2$ (approximately two standard deviations) are generally considered to be statistically significant (Reasenberg and Simpson, 1992; Hill and Prejean, 2007).

The β-statistic approach has been applied to earthquakes listed in the standard catalogs (e.g., Gomberg *et al.*, 2001) or visually identified from high-pass filtered seismograms (Miyazawa and Mori, 2005; Peng *et al.*, 2010). In both cases, each earthquake is treated as the same, and its magnitude (or amplitude in seismogram) information is not been used. According to the well-known Gutenberg and Richter (1944) frequency-magnitude relationship for earthquakes (with a nominal b value of 1), one event with M 3 would correspond to 10 events with M 2 (or 10 events with amplitudes 10 times smaller). Hence, the magnitudes (or amplitudes) of triggered event could play a very important role in determining the β-statistic, which has not been fully explored yet.

Miyazawa and Mori (2005) replaced the number of earthquakes in equation A1 with the amplitude of 5–20 Hz band-pass-filtered envelopes to evaluate remote triggering of nonvolcanic tremor in Japan during the surface waves of the 2003 M 8.3 Tokachi-oki earthquake. Their approach takes into consideration of the amplitude of the seismic waves, and can be applied automatically to identify regions with elevated high-frequency signals that are generated by earthquakes or nonvolcanic tremor. In their study, the number of earthquakes in equation A1 is replaced by the amplitude of the root mean square (rms) envelopes, with the assumption that high-frequency signals are caused by locally triggered activity. Such assumption is best suited for the extremely quiet Hi-Net borehole stations, where the high-frequency signals are less contaminated by near-surface noises (in the forms of either culture noises or caused by natural surface disturbances). However, in our study, most of the stations are placed in the near surface, and hence could be partially contaminated by the near-surface high-frequency noises. In addition, for stations within ~1000 km of the epicenter of the Wenchuan mainshock, some high-frequency signals are caused by the intensive aftershock activity in the mainshock source region immediately after the mainshock. In viewing this, we take a rather conservative approach here by first picking earthquakes from the band-pass-filtered envelopes, followed by a slightly different approach to compute the β-statistic.

We visually identify earthquakes as impulsive seismic energy with clear P and S arrivals on 5-Hz high-pass filtered seismograms and S-P time no more than 15 s (approximately corresponding to a propagating distance of 120 km). The peak amplitude of hand-picked event is then measured from the stacked envelope function. The amplitude of each event needs to be larger than 10 times of the MAD to ensure that the handpick event is not associated with random fluctuations or other near-surface high-frequency noise. Finally, we replace the number of earthquakes n_b and n_a in equation A1 with the amplitude-normalized number N_b and N_a that are computed as follows.

Suppose $A_i (i = 1, 2, \ldots, n_b)$ and $A'_i (i = 1, 2, \ldots, n_a)$ are the peak amplitudes of earthquakes before and after mainshock, and $\hat{A}_b$ is the average amplitude of earthquakes within t_b. We have

$$\hat{A}_b = \frac{1}{n_b} \sum_{i=1}^{n_b} A_i. \tag{A4}$$

The normalized numbers of earthquakes before and after the mainshock are

$$N_b = \frac{1}{\hat{A}_b} \sum_{i=1}^{n_b} A_i = n_b \quad \text{and} \quad N_a = \frac{1}{\hat{A}_b} \sum_{i=1}^{n_a} A'_i. \tag{A5}$$

When there is no earthquake before the mainshock ($n_b = 0$), equation A1 becomes singular. Following Kilb *et al.* (2002), we assign $N_b = n_b = 0.25$, and $\hat{A} = 10b$ MAD to compute N_b.

The aforementioned procedure involves handpicking and hence is somewhat subjective. Therefore, we also include an automatic approach to compute the β-statistic by treating all signals above the threshold as potential seismic signals. The equations are the same as the hand-picked case, except that we exclude the high-frequency signals associated with the P wave of the Wenchuan mainshock and obvious spikes caused by slight clipping or missing of a few data points. In each station, we compute the β-statistic using both the manual and automatic approaches. We only consider stations as triggered significantly when $\beta > 2$ from both approaches are met.

It is well known that the background seismicity could also vary with space and time. Hence, the observed change

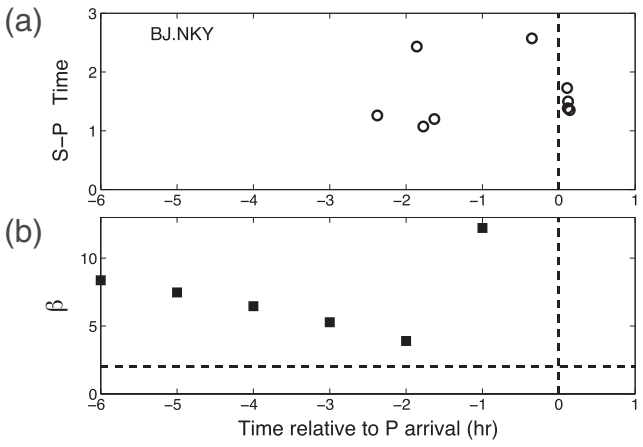

Figure A1. (a) S-P versus the occurrence times of all the hand-picked events at the station BJ.NKY 6 hr before and 1 hr after the predicted P-arrival of the Wenchuan mainshock (vertical dashed line). (b) The corresponding β-values for different time windows before the mainshock. The horizontal dashed line marks the β-value of 2, above which we consider as statistically significant triggering.

in the seismicity rate before and after the mainshock could be contaminated by such random fluctuation in the background seismicity. To evaluate such potential artifact, we vary the time windows before the mainshock from 1 to 6 hr with a step of 1 hr and compute the manual β-values accordingly (Fig. A1 and Ⓔ Table S3, available in the electronic supplement to this paper). The variation in the β-value mainly reflects fluctuation in the background seismicity. We consider a station is less contaminated by the aforementioned fluctuation if the β-values for all the pre-mainshock time windows are larger than 2. More discussions on the findings of this test can be found in the main text.

College of Instrumentation and Electrical Engineering
Jilin University
Changchun, Jilin, China
(T.J., Z.P.)

Institute of Earthquake Science
China Earthquake Administration
Beijing, China
(W.W., Q.-F.C.)

Manuscript received 9 September 2009